Supporting information

Exploring Cation-Deficient Magnetite as a Cathode for Zinc-ion Aqueous Batteries

Akshatha Venkatesha,[1] Gowra Raghupathy Dillip,[1,] [4]Tanmay Mohan Bhagwat,[3]Sayak Mandal,[1]Rekha Kumari,[1,] [2] Martin Etter,[5]Gopalakrishnan Sai Gautam,[3]Aninda J. Bhattacharyya[*, 1, 2]

[1]Solid State and Structural Chemistry Unit, Indian Institute of Science, Bengaluru, 560012, India; [2]Interdisciplinary Centre for Energy Research, Indian Institute of Science, Bengaluru 560012, [3]Department of Materials Engineering, Indian Institute of Science, Bengaluru 560012 India; [4]Energy Institute, Centre of Rajiv Gandhi Institute of Petroleum Technology, Bengaluru 560064, India; [5]Deutsches Elektronen-Synchrotron (DESY), Notkestr. 85 22607 Hamburg, Germany

[*]E-mail: anindajb@iisc.ac.in

Number of pages: 35

Number of figures: 21

Number of tables: 10

Table of Contents:

1. **Figure S1:** TGA of pristine Fe_3O_4, Fe_3O_4-VA-300, Fe_3O_4-VA-400 and Fe_3O_4-VA-500.
2. **Figure S2:** N_2 adsorption-desorption isotherm of (a) pristine Fe_3O_4, (b) Fe_3O_4-VA-300, (c) Fe_3O_4-VA-400 and (d) Fe_3O_4-VA-500.
3. **Figure S3:** Scanning electron micrographs of (a) pristine Fe_3O_4, (b) Fe_3O_4-VA-300, (c)Fe_3O_4-VA-400 and (d) Fe_3O_4-VA-500.

4. **Figure S4:** TEM of (a) pristine Fe_3O_4 and (b) Fe_3O_4-VA-300 and their particle distribution histogram in (c) and (d) respectively. TEM of (e) Fe_3O_4-VA-400 and (f) Fe_3O_4-VA-500 and their particle distribution histogram in (g) and (h) respectively.
5. **Figure S5:** (a) Synchrotron PXRD of Fe_3O_4-VA-300 and Fe_3O_4-VA-400 samples and the Rietveld refinement for the quantification of biphase (b) Laboratory data of Pristine Fe_3O_4, Fe_3O_4-VA-300, Fe_3O_4-VA-400 and Fe_3O_4-VA-500 samples and the Rietveld refinement analysis.
6. **Table S1:** (a) Refinement results of synthesized samples using synchrotron data (b) Refinement results of synthesized samples using laboratory data.
7. **Figure S6:** Raman spectra of Fe_3O_4-VA-300 and Fe_3O_4-VA-400 samples exhibit signature bands corresponding to Fe-O bonds of Fe_3O_4.
8. **Figure S7:** FTIR of pristine Fe_3O_4, Fe_3O_4-VA-300, Fe_3O_4-VA-400, and Fe_3O_4-VA-500
9. **Figure S8:** XPS survey scans of (a) pristine Fe_3O_4, (b) Fe_3O_4-VA-300, (c) Fe_3O_4-VA-400 and (d) Fe_3O_4-VA-500 samples.
10. **Table S2:** Comparison of XPS results of all the samples – Binding energies of Fe and O, FWHM, relative at%, O/Fe, and Fe^{3+}/Fe^{2+} ratios.
11. **Figure S9:** (a) R space plots and (b) k2 weighted Fe K-edge EXAFS oscillations of pristine Fe_3O_4 and all the annealed samples.
12. **Table S3:** The EXAFS fitting results for Pristine Fe_3O_4, Fe_3O_4-VA-300, and Fe_3O_4-VA-400.
13. **Figure S10:** CV of Pristine and annealed Fe_3O_4 samples – (a) 1st cycle and (b) 2nd cycle.
14. **Figure S11:** (a) Long cyclability data of Zn-Fe_3O_4-VA-400 cell (b) Rate capability and coulombic efficiency of Zn-Fe_3O_4-VA-400 cell at various current densities.

15. **Figure S12:** (a) CV of Zn-pristine Fe_3O_4 cell in 1 M $ZnSO_4$ at various scan rates, (b) plot of Log (I_{pa}) versus Log (scan rate), and (c) Log (I_{pc}) versus Log (scan rate).
16. **Figure S13:** (a) CV of Zn-Fe_3O_4-VA-400 cell in 1 M $ZnSO_4$ at various scan rates, (b) plot of Log (I_{pa}) versus Log (scan rate), and (c) Log (I_{pc}) versus Log (scan rate).
17. **Section S1:** Determining the percentage contribution of diffusion-controlled and pseudocapacitive storage mechanisms in Zn-pristine Fe_3O_4 and Zn-Fe_3O_4-VA-400 cells.
18. **Figure S14:** Plots of (a) $I_{pa}/v^{1/2}$ versus $v^{1/2}$and (b) $I_{pc}/v^{1/2}$ versus $v^{1/2}$ of Zn-pristine Fe_3O_4 cell in 1 M $ZnSO_4$
19. **Figure S15:** Plots of (a) $I_{pa}/v^{1/2}$ versus $v^{1/2}$and (b) $I_{pc}/v^{1/2}$ versus $v^{1/2}$ of Zn- Fe_3O_4-VA-400 cell in 1 M $ZnSO_4$
20. **Table S4:** Values showing % contributions from diffusion and pseudocapacitance in Zn-pristine Fe_3O_4 and Zn-Fe_3O_4-VA-400 cells.
21. **Figure S16:** (a) and (b) Nyquist plots, before cycling and after the 10th discharge for Zn-pristine Fe_3O_4 and Zn-Fe_3O_4-VA-400 cells. (c) and (d) GITT plots for Zn-pristine Fe_3O_4 and Zn-Fe_3O_4-VA-400 cells.
22. **Figure S17:** (a and b) PXRD of pristine Fe_3O_4 and Fe_3O_4-VA-400 before and after various cycling stages.
23. **Figure S18:** (a-d) XPS spectra of Fe 2p, O1s, Zn 2p, and S 2p of pristine Fe_3O_4 electrodes before cycling, after 1st discharge, and 1st charge, respectively (bottom to top).
24. **Figure S19:** (a-d) XPS spectra of Fe 2p, O1s, Zn 2p, and S 2p of Fe_3O_4-VA-300 electrodes before cycling, after 1st discharge, and 1st charge, respectively (bottom to top).

25. **Figure S20:** (a-d) XPS spectra of Fe 2p, O1s, Zn 2p, and S 2p of Fe_3O_4-VA-500 electrodes before cycling, after 1st discharge, and 1st charge, respectively (bottom to top).
26. **Table S5:** Comparison of XPS results before and after cycling of the cells and their peak binding energy, FWHM, relative at%, O/Fe, and Fe^{3+}/Fe^{2+} ratios.
27. **Figure S21:** (a and c) Comparison of EXAFS (R-space) data of pristine Fe_3O_4, Fe_3O_4-VA-300, and Fe_3O_4-VA-500 before and after cycling, (b) Experimental EXAFS (R-space) data and the fitting using theoretical model for Fe_3O_4-VA-300
28. **Table S6:** Amplitude reduction factor (S_0^2), correction to edge energy (ΔE_0), coordination number (N), path distance (R), pseudo/EXAFS Debye–Waller factor (σ^2) of the different scattering paths obtained from the EXAFS data fitting of the pristine Fe_3O_4 sample: (A), (B), and (C) – Before cycling, after 1st discharge, and after 1st charge.
29. **Table S7:** Fitting results (S_0^2, ΔE_0, N, R, and σ^2) obtained from the EXAFS data fitting of the Fe_3O_4-VA-300 sample: (A), (B), and (C) – Before cycling, after 1st discharge, and after 1st charge.
30. **Table S8:** Fitting results (S_0^2, ΔE_0, N, R, and σ^2) obtained from the EXAFS data fitting of the Fe_3O_4-VA-400 sample: (A), (B), and (C) – Before cycling, after 1st discharge, and after 1st charge.
31. **Table S9:** Lattice parameter as obtained from the EXAFS data fitting.
32. **Table S10:** Density functional theory (DFT) calculated reaction enthalpies, represented as voltages versus Zn metal, for possible conversion reactions of Zn with stoichiometric Fe_3O_4 and intercalation into Fe-deficient $Fe_{22}O_{32}$. Voltage for a given reaction equals the negative of reaction enthalpy (in eV) normalized by the 2 × number

of Zn atoms as a reactant and the Faraday constant. Positive reaction voltage indicates spontaneity. Reaction in bold is most spontaneous.

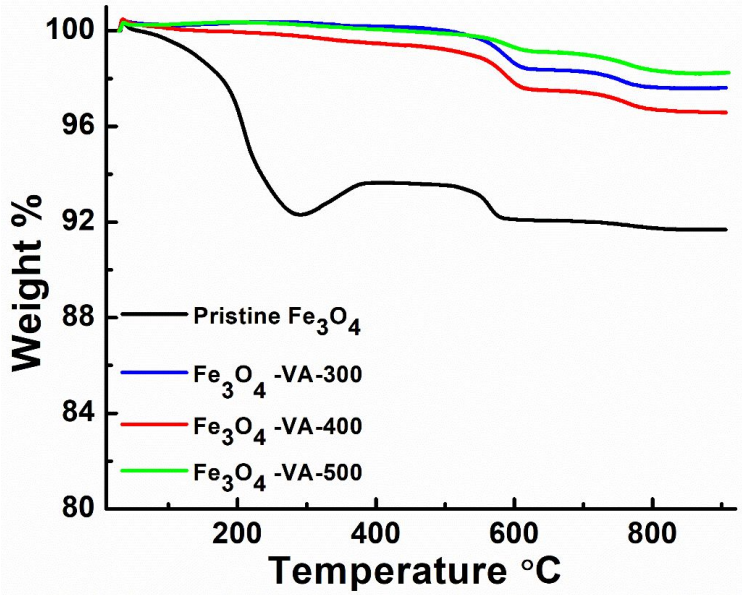

Figure S1: Thermogravimetric analysis (TGA) of all samples in the N_2 atmosphere. The initial weight loss of 5% seen in the pristine Fe_3O_4 starting from 150 - 200˚C is due to the loss of adsorbed water molecules trapped in the crystal structure (black color line). After 200˚C, the weight loss in the material can be attributed to the phase transformation. After 400˚C, the material is stable up to 550˚C, after which a second weight loss is seen. In the case of Fe_3O_4-VA-300 (blue color, line), the material is found to be thermally stable up to 550˚C, after which the material starts degrading. Similar thermal stability features are seen in Fe_3O_4-VA-400 and Fe_3O_4-VA-500 (red and green color lines, respectively).

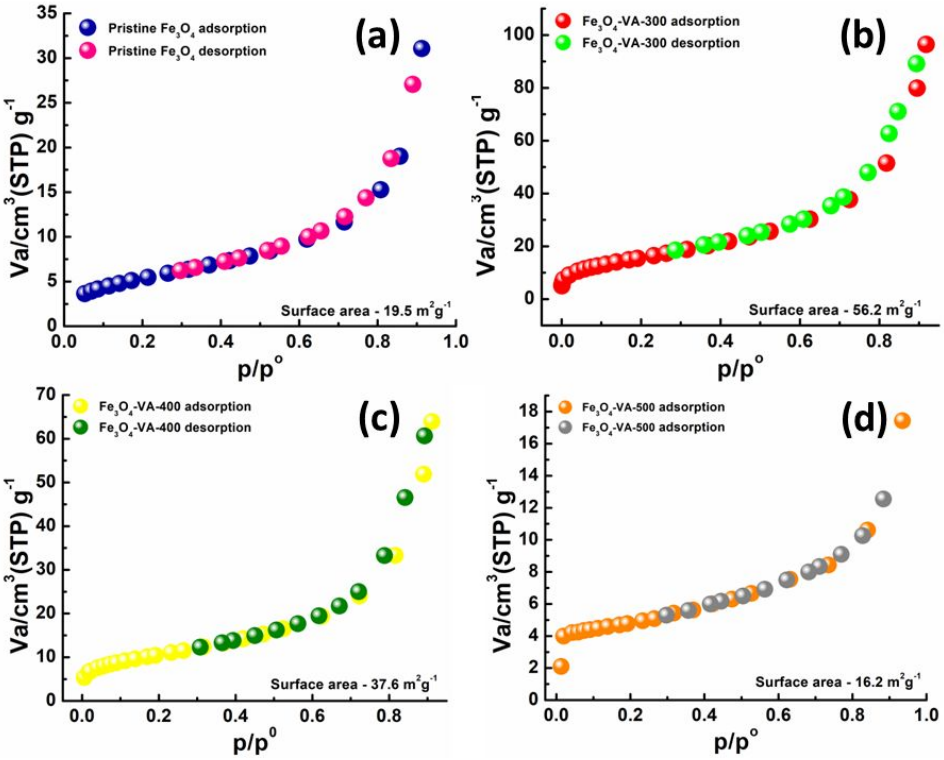

Figure S2: N_2 adsorption-desorption isotherms (Type II) of nonporous samples. The Brunauer–Emmett–Teller (BET) surface area of (a) pristine Fe_3O_4, (b) Fe_3O_4-VA-300, (c) Fe_3O_4-VA-400, and (d) Fe_3O_4-VA-500 are estimated to be 19.5, 56.2, 37.6, and 16.2 m^2g^{-1} respectively.

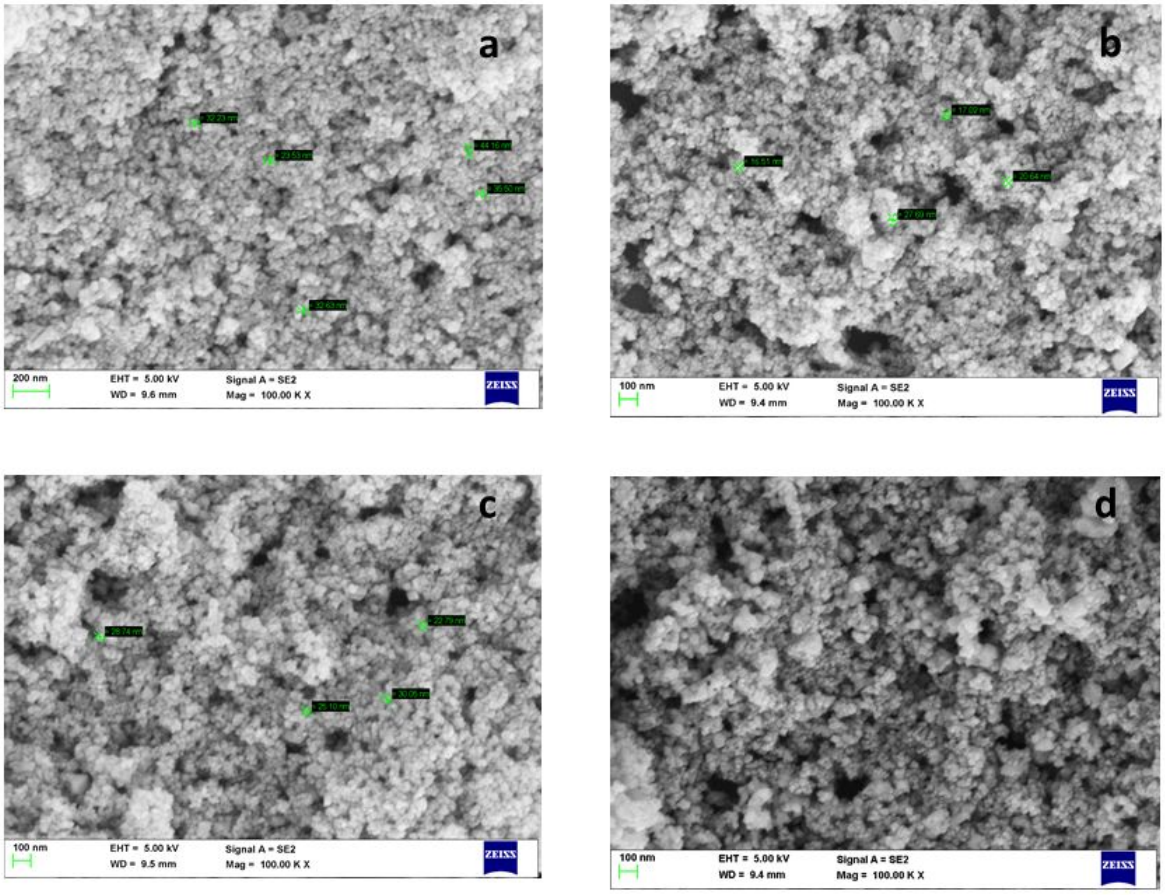

Figure S3: SEM of (a) pristine Fe_3O_4, (b) Fe_3O_4-VA-300, (c) Fe_3O_4-VA-400, and (d) Fe_3O_4-VA-500.

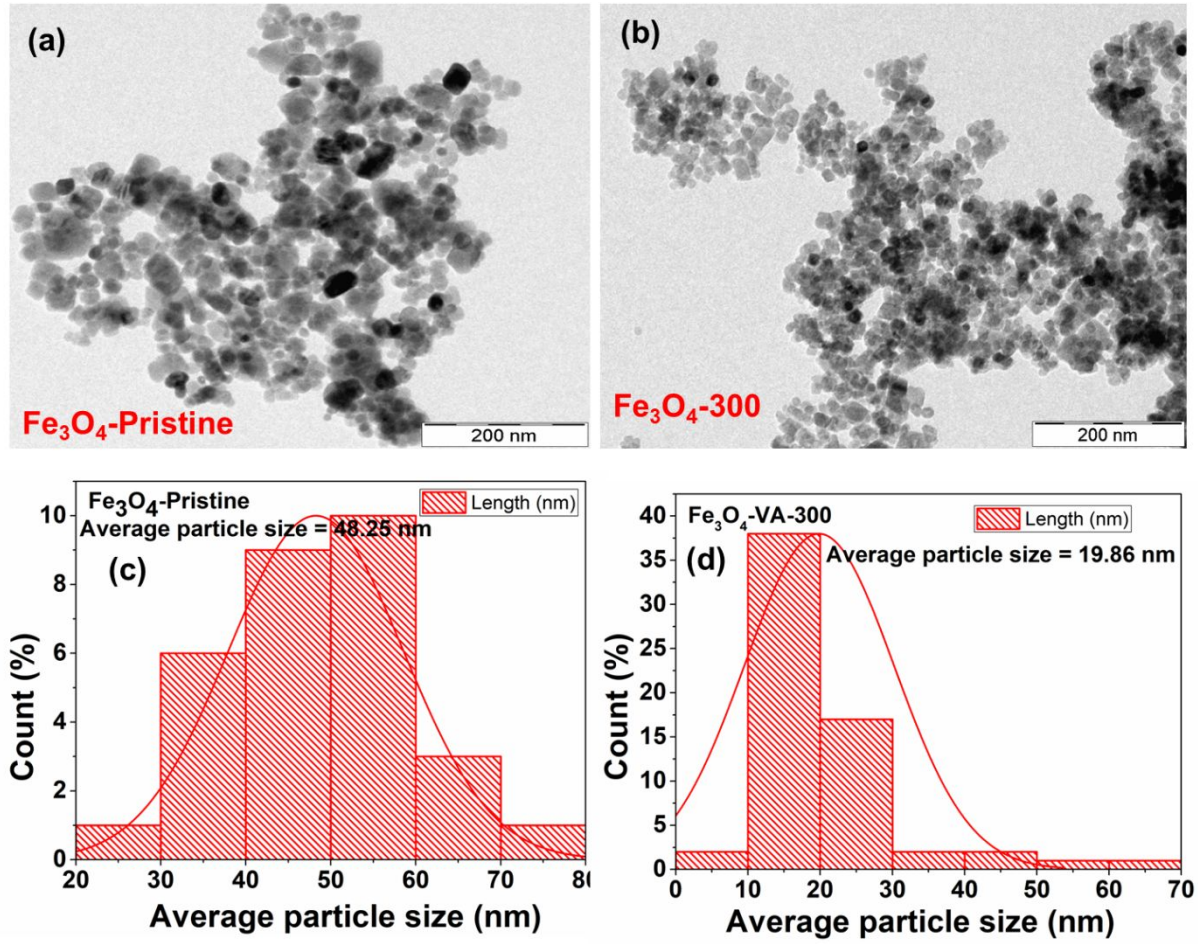
(a)
Fe3O4-Pristine
200 nm
(b)
Fe3O4-300
200 nm
Fe3O4-Pristine
Average particle size = 48.25 nm
(c)
Length (nm)
Count (%)
Average particle size (nm)
Fe3O4-VA-300
Average particle size = 19.86 nm
(d)
Length (nm)
Count (%)
Average particle size (nm)

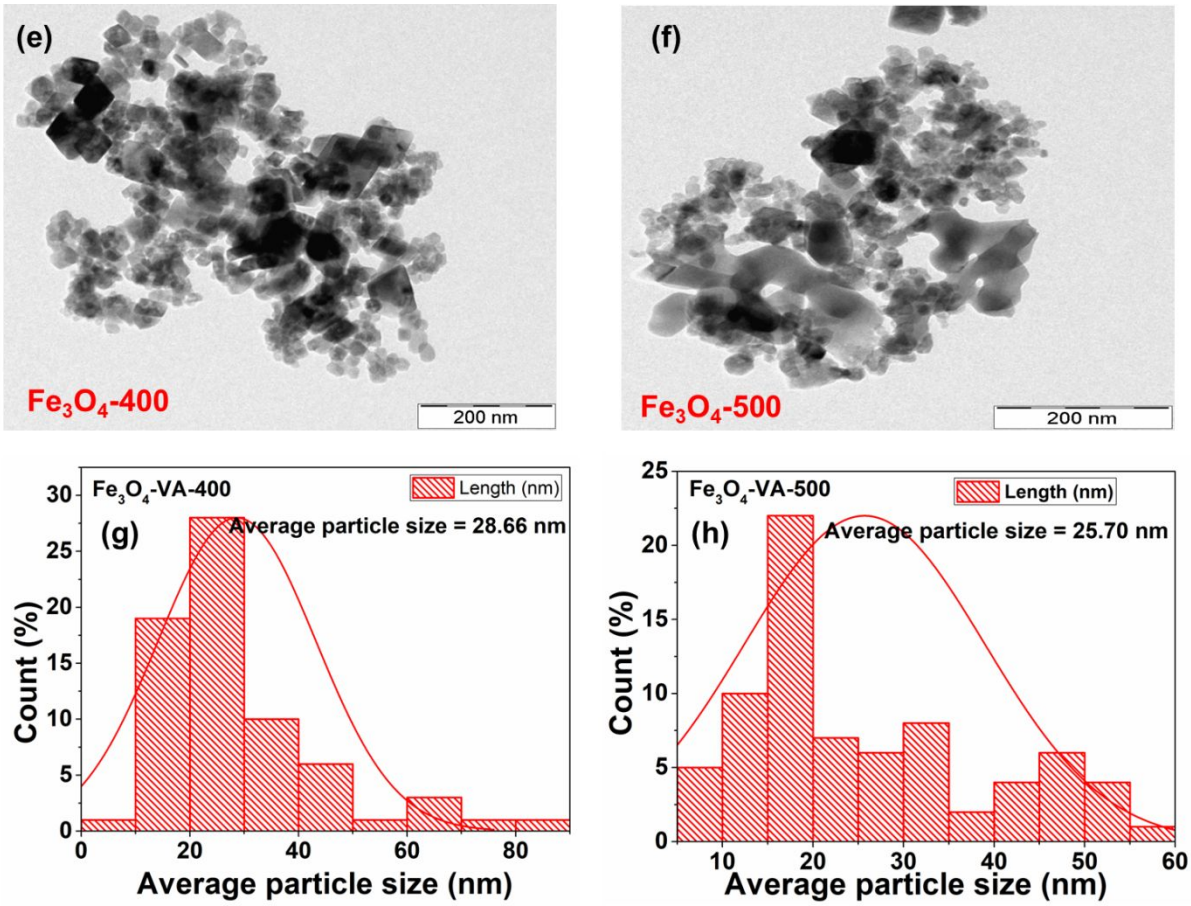

Figure S4: TEM of (a) pristine Fe_3O_4 and (b) Fe_3O_4-VA-300 and their particle distribution histogram in (c) and (d) respectively. TEM of (e) Fe_3O_4-VA-400 and (f) Fe_3O_4-VA-500 and their particle distribution histogram in (g) and (h) respectively.

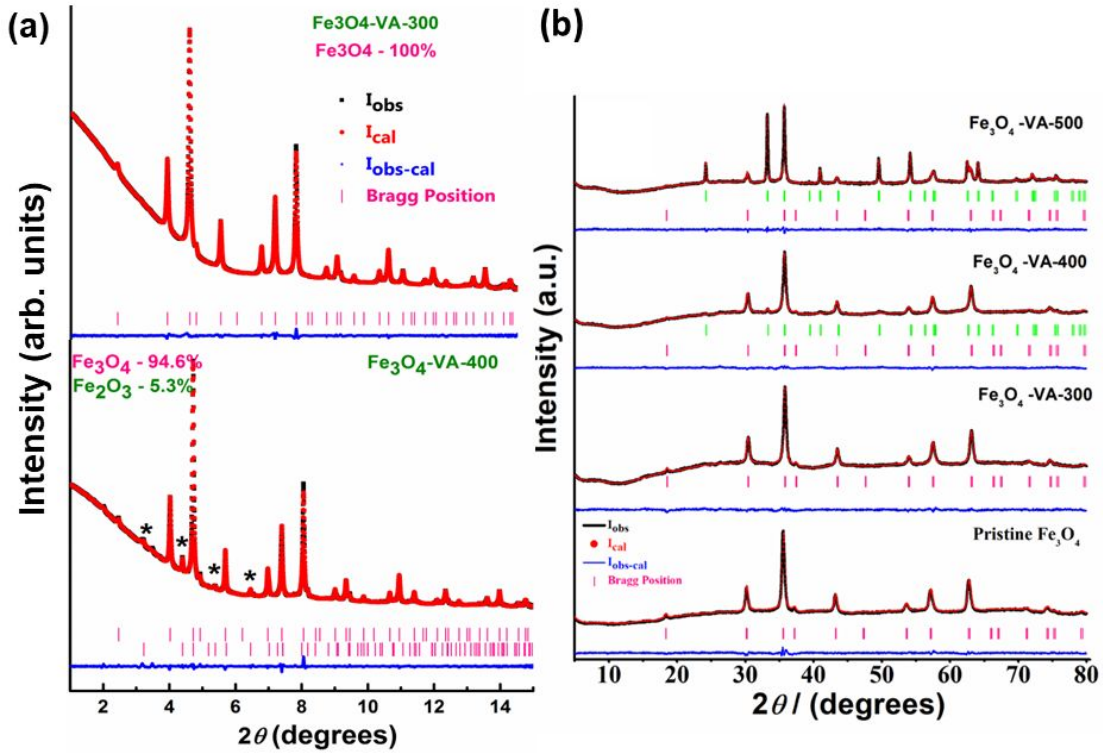

Figure S5 (a): Synchrotron PXRD of Fe_3O_4-VA-300, Fe_3O_4-VA-400 samples. Fe_3O_4-VA-300 possesses a single magnetite phase only, while Fe_3O_4-VA-400 has two phases: magnetite and hematite **(b):** PXRD of Fe_3O_4, Fe_3O_4-VA-300, Fe_3O_4-VA-400, and Fe_3O_4-VA-500samples. Fe_3O_4-VA-300 possesses a single magnetite phase only, while Fe_3O_4-VA-400 has two phases: magnetite and hematite.

Table S1: (a) X-ray diffraction refinement results of synthesized samples using the synchrotron diffractometer.

Sample	Space group	Unit cell parameters				Position parameters					Phase %	R-factors			Chi 2
		a **(Å)**	***b*** **(Å)**	***c*** **(Å)**	***V*** **(Å)³**	**Atom**	**Occupancy**	***x***	***y***	***z***		R_{exp}	R_p	R_{wp}	
Pristine Fe_3O_4	F d -3 m (227)	8.36 (1)	8.36 (1)	8.36 (1)	585.76	Fe1	0.94	0.375	0.375	0.375	100	0.66	0.95	1.71	6.60
						Fe2	0.86	0	0	0					
						O1	1.0	0.246	0.246	0.246					
Fe_3O_4-VA-300	F d -3 m (227)	8.34 (1)	8.34 (1)	8.34 (1)	580.20	Fe1	0.90	0.375	0.375	0.375	100	0.68	0.54	0.96	1.99
						Fe2	0.78	0	0	0					
						O1	1.0	0.246	0.246	0.246					
Fe_3O_4-VA-400	F d -3 m (227)	8.34 (1)	8.34 (1)	8.34 (1)	580.59	Fe1	0.91	0.375	0.375	0.375	94.62	0.68	0.71	1.17	2.93
						Fe2	0.77	0	0	0					
						O1	1.0	0.246	0.246	0.246					
	R -3 c (167)	5.03 (5)	5.03 (5)	13.73 (1)	301.34	Fe1	1.0	0	0	0.145	5.38				
						O1	1.0	0.299	0	0.25					
Fe_3O_4-VA-500	F d -3 m (227)	8.34 (2)	8.34 (2)	8.34 (2)	581.35	Fe1	0.95	0.375	0.375	0.375	27.74	1.11	1.66	3.09	7.72
						Fe2	0.83	0	0	0					
						O1	1.0	0.246	0.246	0.246					
	R -3 c (167)	5.03 (6)	5.03 (6)	13.74 (2)	301.62	Fe1	0.95	0	0	0.145	72.26				
						O1	1.0	0.305	0	0.25					

Table S1: (b) X-ray diffraction refinement results of synthesized samples using the laboratory diffractometer.

Sample	Phase	Space group	Unit cell parameters				Position parameters					Phase %	R-factors			GOF
			a (Å)	*b* (Å)	*c* (Å)	*V* (Å)^3	Atom	Occupancy	*x*	*y*	*z*		R_{exp}	R_p	R_{wp}	
Pristine Fe_3O_4	$Fe_{22.51}O_{32}$	F d -3 m (227)	8.37 (4)	8.37 (4)	8.37 (4)	587.41	Fe1	0.99	0.375	0.375	0.375	100	0.46	0.48	0.67	2.13
							Fe2	0.91 (2)	0	0	0					
							O1	1	0.245	0.245	0.245					
Fe_3O_4-VA-300	$Fe_{22.91}O_{32}$	F d -3 m (227)	8.34 (4)	8.34 (4)	8.34 (4)	581.34	Fe1	1	0.375	0.375	0.375	100	0.47	0.43	0.57	1.43
							Fe2	0.93	0	0	0					
							O1	1	0.245	0.245	0.245					
Fe_3O_4-VA-400	$Fe_{22.01}O_{30.74}$	F d -3 m (227)	8.35 (5)	8.35 (5)	8.35 (5)	581.36	Fe1	1	0.375	0.375	0.375	94.8	0.48	0.47	0.59	1.55
							Fe2	0.87 (2)	0	0	0					
							O1	0.96	0.245	0.245	0.245					
	$Fe_{12}O_{18}$	R -3 c (167)	5.04 (2)	5.04 (2)	13.73 (7)	301.39	Fe1	1	0	0	0.144	5.2				
							O1	1	0.305	0	0.25					
Fe_3O_4-VA-500	$Fe_{23.66}O_{29.65}$	F d -3 m (227)	8.35 (4)	8.35 (4)	8.35 (4)	581.57	Fe1	0.99 (5)	0.375	0.375	0.375	34.1	0.49	0.48	0.64	1.69
							Fe2	0.97	0	0	0					
							O1	0.92	0.245	0.245	0.245					
	$Fe_{12}O_{18}$	R -3 c (167)	5.03 (1)	5.03 (1)	13.73 (7)	301.73	Fe1	1	0	0	0.144	65.9				
							O1	1	0.305	0	0.25					

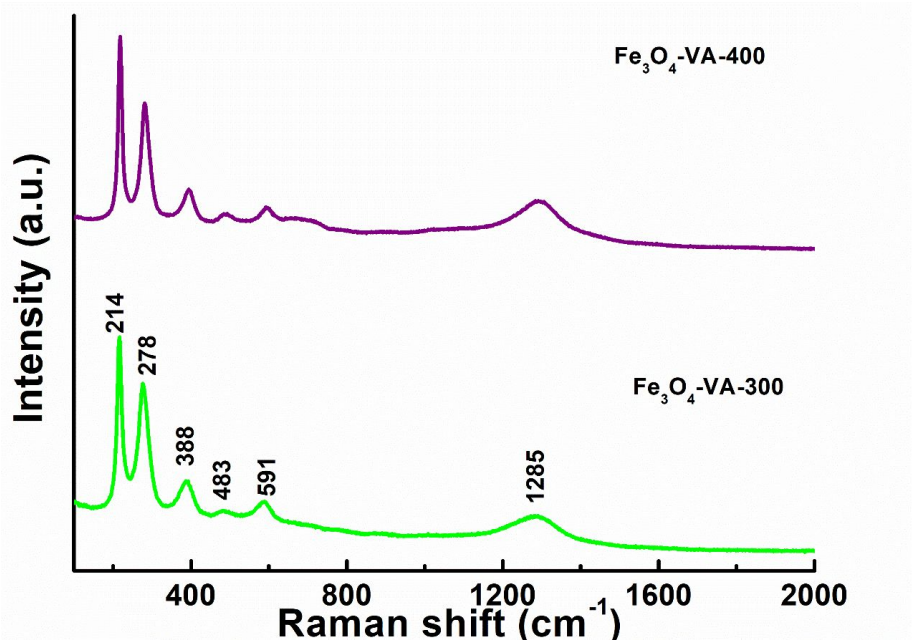

Figure S6: Raman spectra of Fe_3O_4-VA-300 and Fe_3O_4-VA-400 samples exhibit signature bands corresponding to Fe-O bonds of Fe_3O_4.

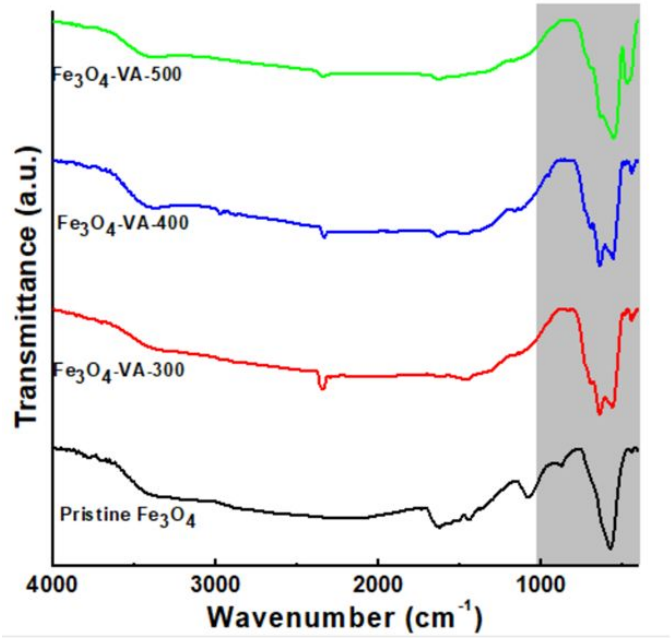

Figure S7: Fourier transform Infrared (FTIR) spectroscopy of pristine and annealed Fe_3O_4 samples. The IR spectra of all four samples show a broad hump-like band around 3430 cm^{-1} attributed to O-H stretching of physi-adsorbed water molecules. The surface hydroxyl groups decreased in the vacuum-annealed samples compared to the RT sample. IR peak at around 2340 cm^{-1} in all the samples corresponds to asymmetric stretching of CO_2. The IR peaks ranging from 635 cm^{-1} to 550 cm^{-1} originate from the Fe-O vibrations.

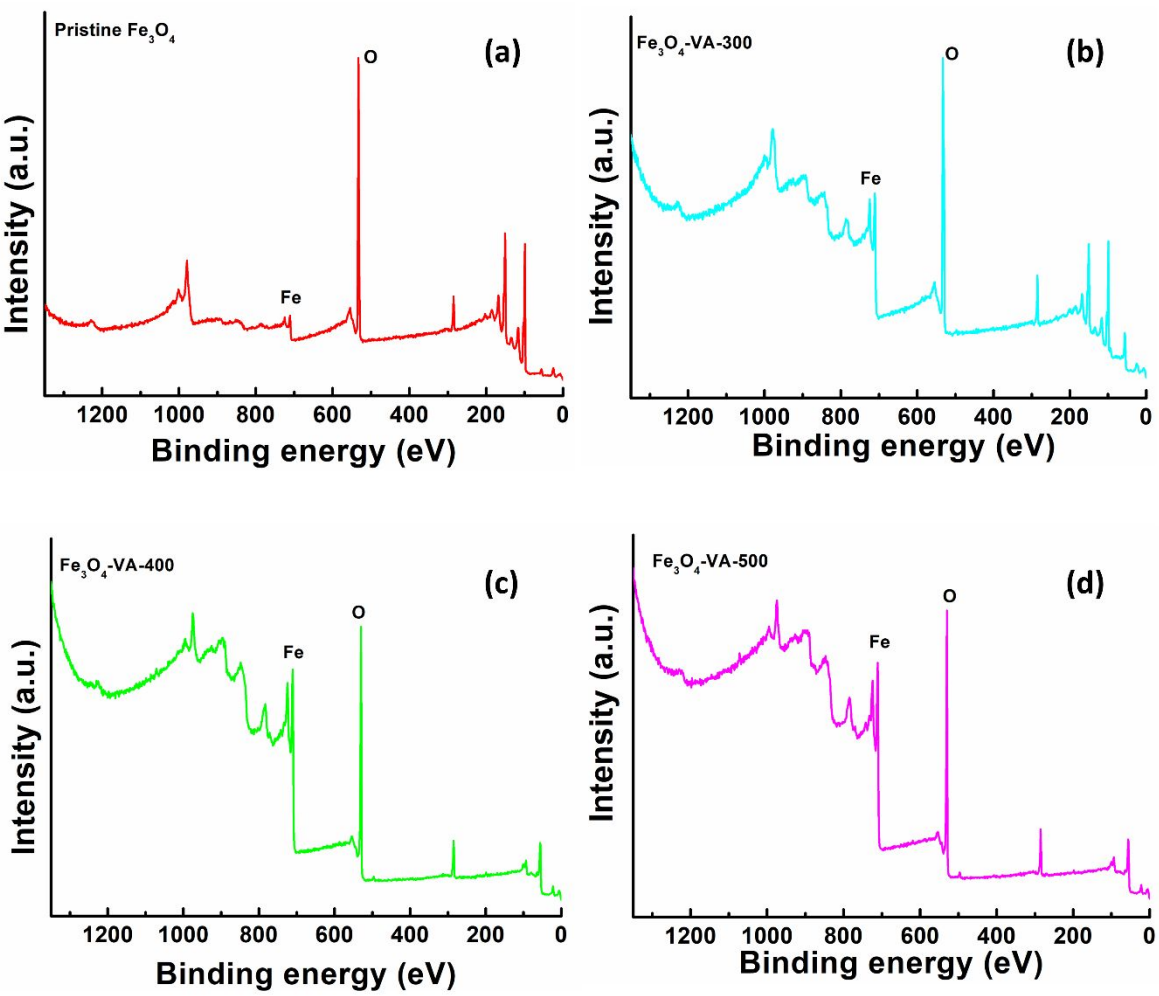

Figure S8: XPS survey scans of (a) pristine Fe_3O_4, (b) Fe_3O_4-VA-300, (c) Fe_3O_4-VA-400 and (d) Fe_3O_4-VA-500 samples.

Table S2: Comparison of XPS results of all the samples – binding energies of Fe and O, FWHM, relative at%, O/Fe, and Fe^{3+}/Fe^{2+} ratios.

Sample	Peak binding energy (eV±0.2) / [FWHM (eV)]/ (relative at (%))							Elemental at%		Ratio	
	O 1*s*			Fe 2*p*				O	Fe	O/Fe	Fe^{3+}/Fe^{2+}
				Fe^{2+}		Fe^{3+}					
	O1	O2	O3	Fe1	Fe2	Fe3	Fe4				
Pristine Fe_3O_4	530.0 [1.32] (6.13)	-	532.4 [1.32] (89.62)	710.5 [3.01] (2.95)	723.7	713.7 [3.5] (1.3)	727.1	95.75	4.25	1.44	0.44
Fe_3O_4-VA-300	529.8 [1.55] (28.03)	531.5 [1.55] (8.62)	532.7 [1.55] (47.52)	710.5 [2.58] (10.01)	723.7	713.4 [3.5] (5.8)	726.6	84.17	15.83	2.31	0.57
Fe_3O_4-VA-400	529.9 [1.55] (55.04)	531.4 [1.55] (9.79)	532.8 [1.55] (4.48)	710.5 [2.5] (18.85)	723.7	713.3 [3.5] (11.82)	726.5	69.32	30.67	2.11	0.62
Fe_3O_4-VA-500	529.8 [1.54] (54.68)	531.4 [1.54] (9.77)	532.7 [1.54] (5.19)	710.4 [2.41] (17.62)	723.7	713.1 [3.5] (12.72)	726.4	69.65	30.35	2.12	0.72

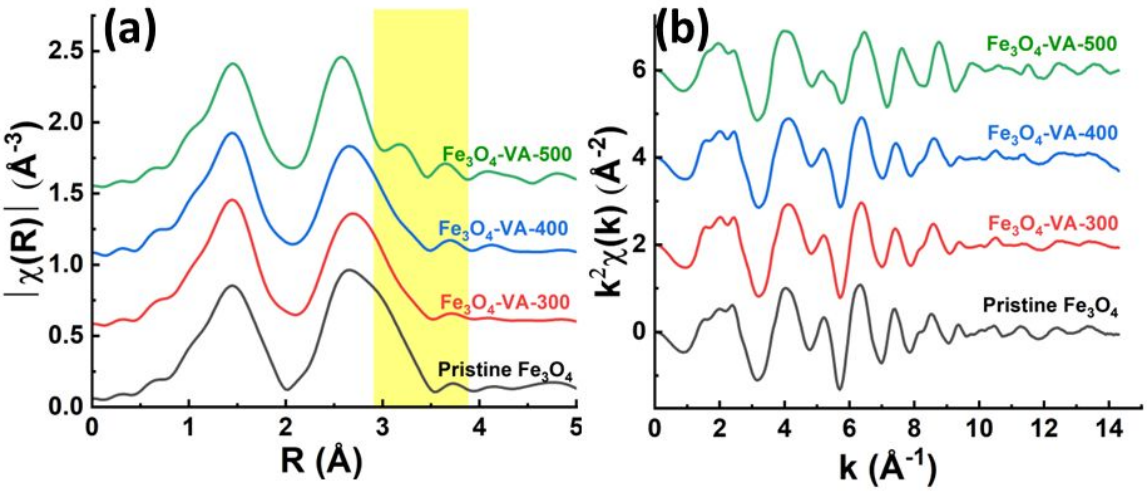

Figure S9: (a) R space plots and (b) k2weighted Fe K-edge EXAFS oscillations of pristine Fe_3O_4 and all the annealed samples.

Table S3: The EXAFS fitting results for pristine Fe_3O_4, Fe_3O_4-VA-300, and Fe_3O_4-VA-400.

Scattering Paths	**Samples**								
	Pristine Fe_3O_4			**Fe_3O_4-VA-300**			**Fe_3O_4-VA-400**		
	N	**R (Å)**	**σ^2 (Å^2)**	**N**	**R (Å)**	**σ^2 (Å^2)**	**N**	**R (Å)**	**σ^2 (Å^2)**
Fe - O	5.95 ± 0.17	1.9661 ± 0.0060	0.0143	5.46 ± 0.17	1.9343 ± 0.0074	0.0119	5.46 ± 0.19	1.9329 ± 0.0080	0.0122
Fe_{Oct} – Fe_{Oct}	4.37 ± 0.30	2.9862 ± 0.0071	0.0120	4.02 ± 0.41	2.9831 ± 0.0089	0.0132	3.53 ± 0.37	2.9731 ± 0.0094	0.0119
$Fe_{Oct/Tetra}$ – $Fe_{Tetra/Octa}$	7.89 ± 0.36	3.4725 ± 0.0069	0.0105	7.35 ± 0.49	3.4455 ± 0.0093	0.0119	6.59 ± 0.51	3.4402 ± 0.0105	0.0119

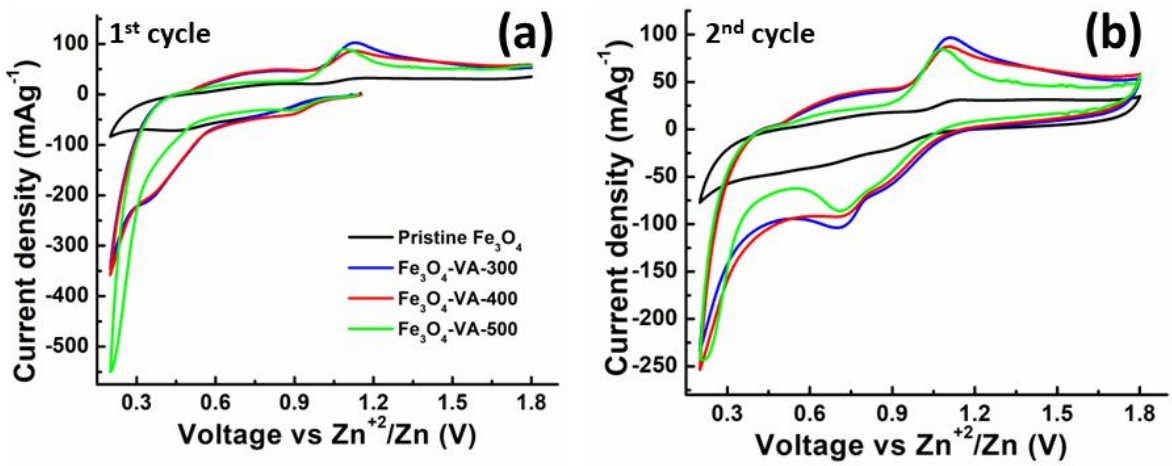

Figure S10: CV of pristine and annealed Fe_3O_4 samples (a) 1st cycle and (b) 2nd cycle at 0.5 mV s^{-1} scan rate.

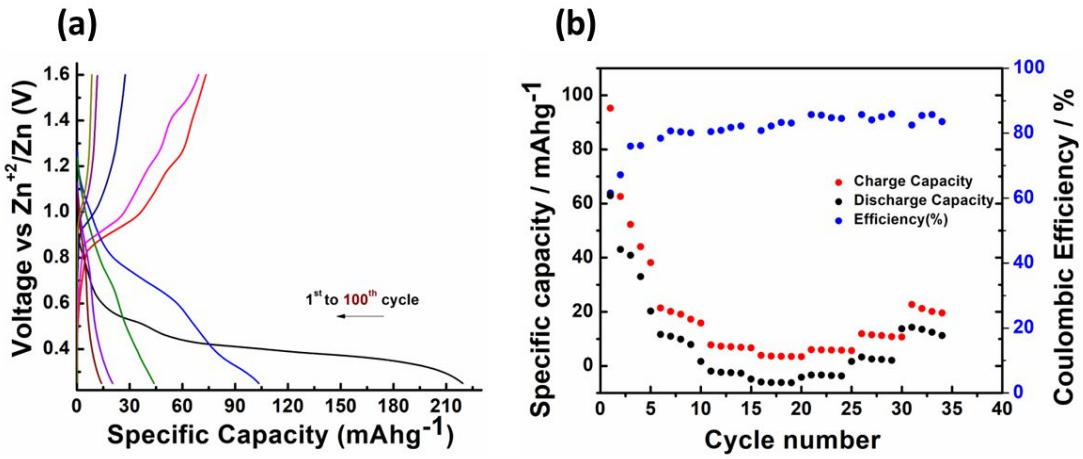

Figure S11: (a) Long cyclability data of Zn-Fe_3O_4-VA-400 cell (b) Rate capability and coulombic efficiency of Zn-Fe_3O_4-VA-400 cell at 12.5, 25, 50 and 100 mAg^{-1} current densities.

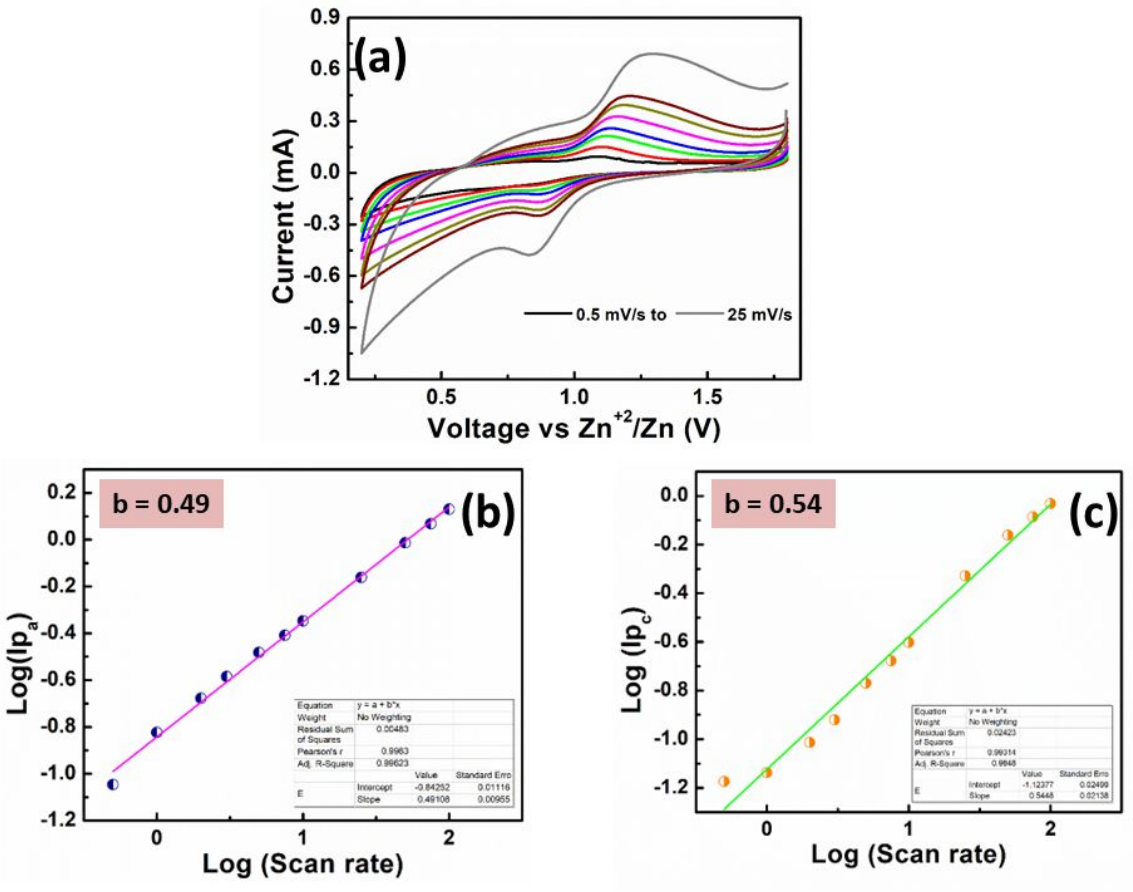

Figure S12: (a) CV at various scan rates, (b) plot of log (I_{pa}) vs. log (scan rate), and (c) log (I_{pc}) vs. log (scan rate) of Zn-pristine Fe_3O_4 cell in 1 M $ZnSO_4$.

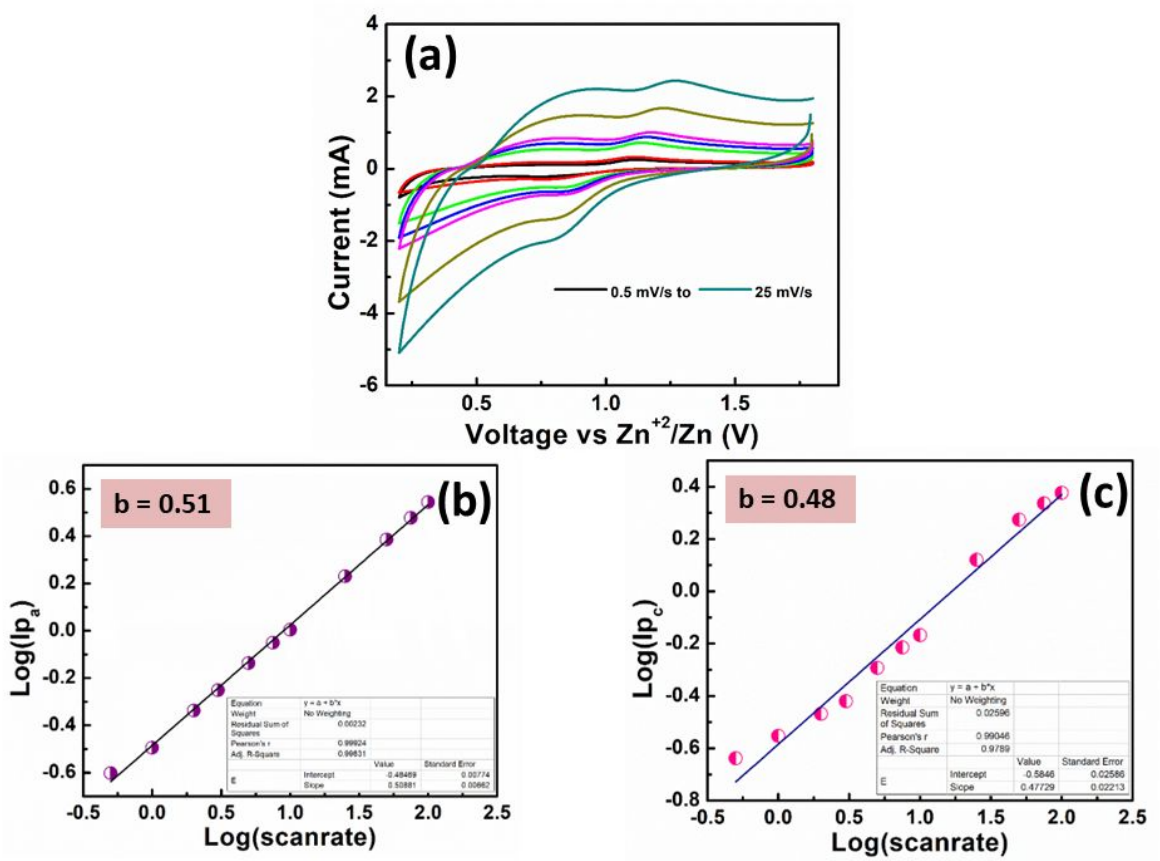

Figure S13: (a) CV at various scan rates, (b) plot of log (I_{pa}) vs. log (scan rate), and (c) log (I_{pc}) vs. log (scan rate) of Zn- Fe_3O_4-VA-400 cell in 1 M $ZnSO_4$.

S1 – Determination of the percentage contribution of diffusion-controlled mechanism and pseudocapacitive storage mechanism in Zn-pristine Fe_3O_4 and Zn-Fe_3O_4-VA-400 cells:

The reaction mechanism occurring at the electrodes can be either due to a diffusion-controlled process or pseudocapacitive storage. In addition to these two processes, there can be the contribution of both types, which might enhance the electrochemical performance of the cell. Thus, the following equation is used to differentiate and quantify the individual type of redox processes.

$$I_p = a\,\upsilon^{1/2} + b\,\upsilon \qquad \text{s1}$$

Where I_p is peak current, I_{pa} is the anodic peak current, and I_{pc} is the cathodic peak current, a and b give the contribution from diffusion and pseudocapacitance, respectively

On dividing the above equation into both sides by $\upsilon^{1/2}$, we get,

$$I_p/\upsilon^{1/2} = a + b\upsilon^{1/2} \qquad \text{s2}$$

Further, the plots of $I_p/\upsilon^{1/2}$ versus $\upsilon^{1/2}$ give intercept a, a fraction of the contribution from the diffusion-controlled process, and slope b gives the contribution of the pseudocapacitive storage phenomenon.

The average % contributions from diffusion and pseudocapacitance are calculated from anodic and cathodic peak currents, as shown in Table S3.

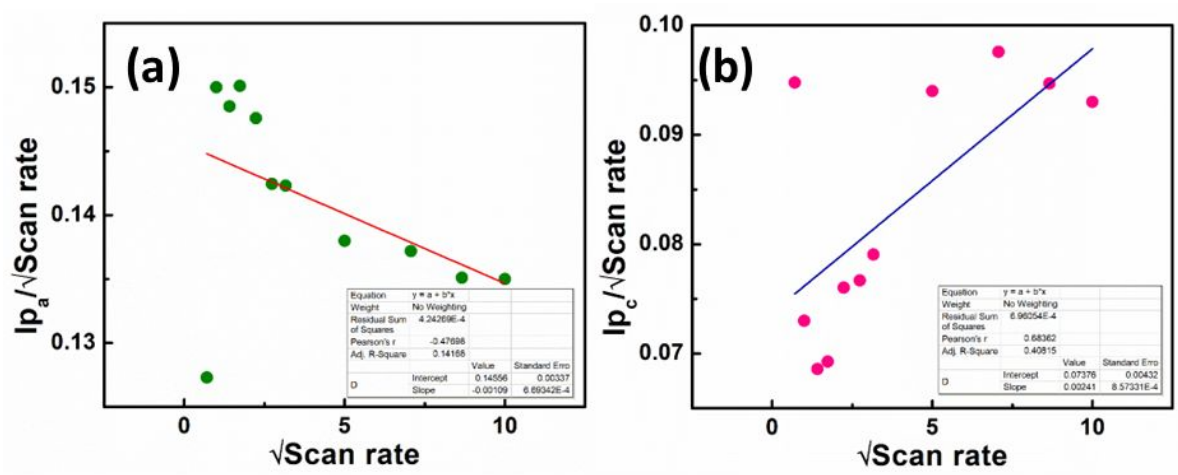

Figure S14: Plots of (a) $I_{pa}/v^{1/2}$ versus $v^{1/2}$ and (b) $I_{pc}/v^{1/2}$ versus $v^{1/2}$ of Zn-pristine Fe_3O_4 cell in 1 M $ZnSO_4$.

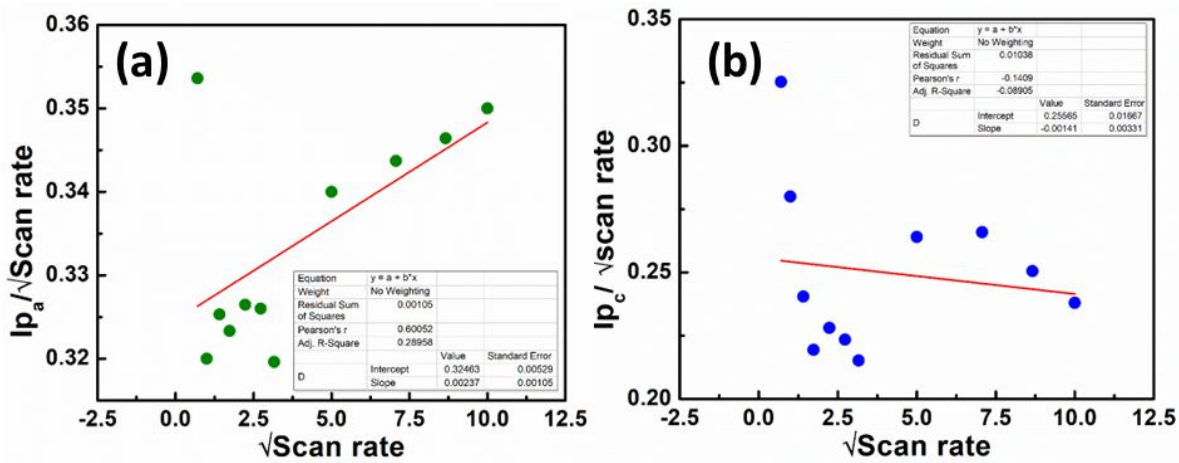

Figure S15: Plots of (a) $I_{pa}/v^{1/2}$ versus $v^{1/2}$and (b) $I_{pc}/v^{1/2}$ versus $v^{1/2}$ of Zn- Fe_3O_4-VA-400 cell in 1 M $ZnSO_4$.

Table S4: Values showing % contributions from diffusion and pseudocapacitance in Zn-pristine Fe_3O_4 and Zn-Fe_3O_4-VA-400 cell

Cell	% Contribution from diffusion	% Contribution from pseudocapacitance
Zn-pristine Fe_3O_4	97.9	2.1
Zn-Fe_3O_4-VA-400	99.6	0.4

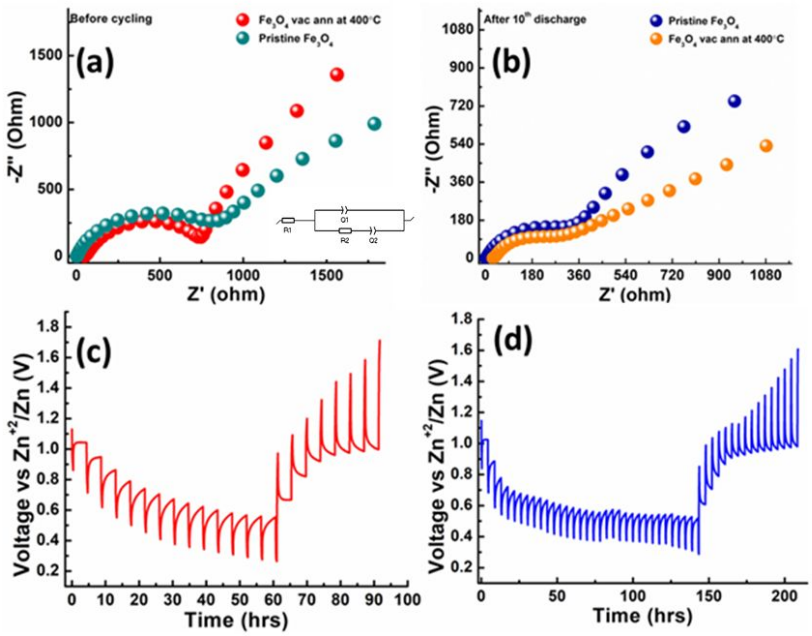

Figure S16: (a) and (b) Nyquist plots, before cycling and after the 10th discharge for Zn-pristine Fe_3O_4 and Zn-Fe_3O_4-VA-400 cells. (c) and (d) GITT plots for Zn-pristine Fe_3O_4 and Zn-Fe_3O_4-VA-400 cells.

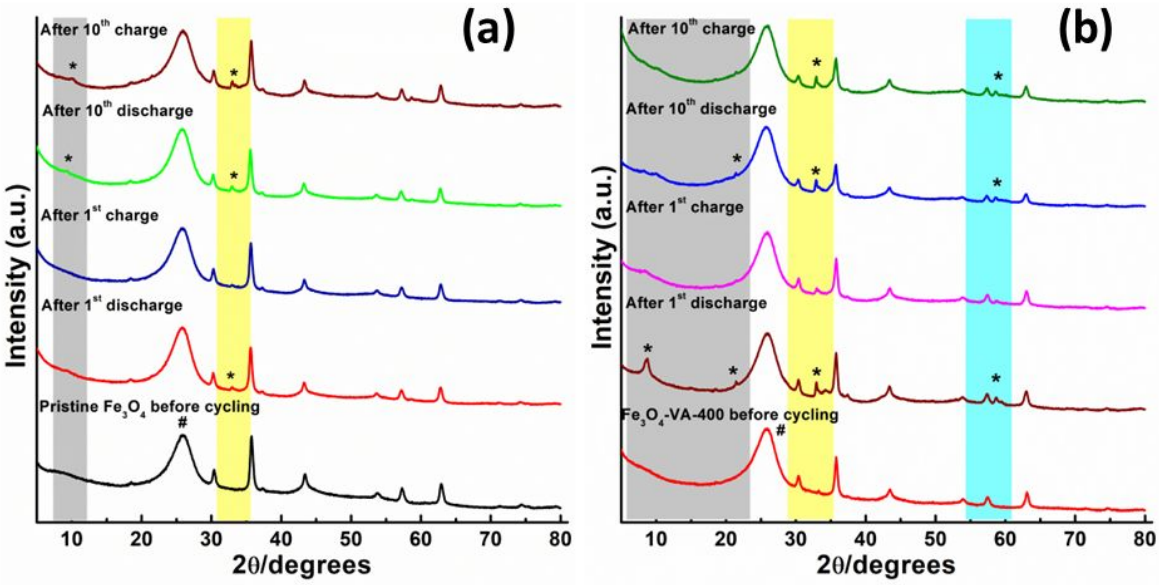

Figure S17: PXRD of pristine Fe_3O_4 (a) and Fe_3O_4-VA-400 (b) before cycling and after various stages of cycling.

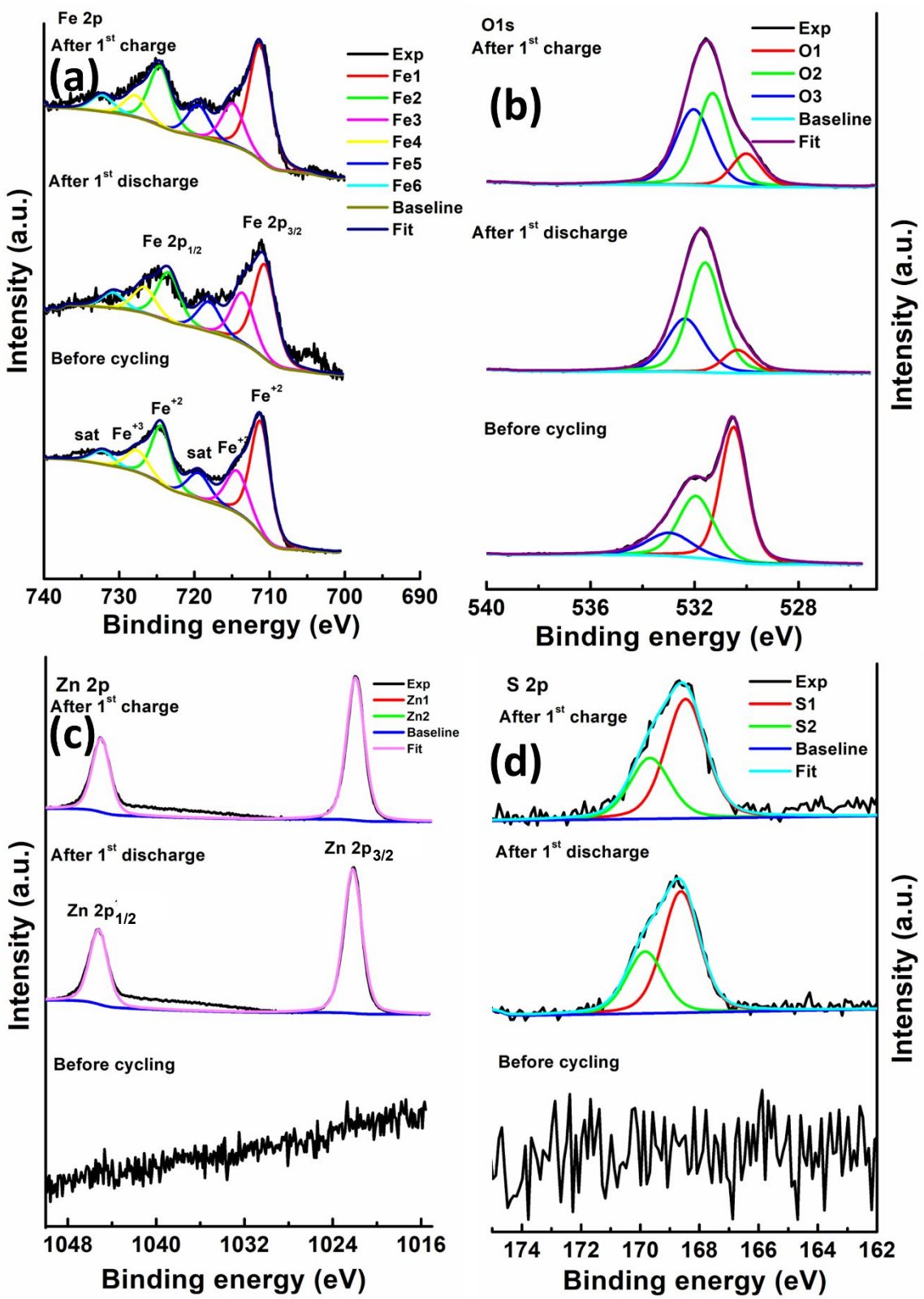

Figure S18: (a-d) XPS spectra of Fe 2p, O1s, Zn 2p, and S 2p of pristine Fe_3O_4 electrodes before cycling, after 1st discharge, and 1st charge, respectively (bottom to top).

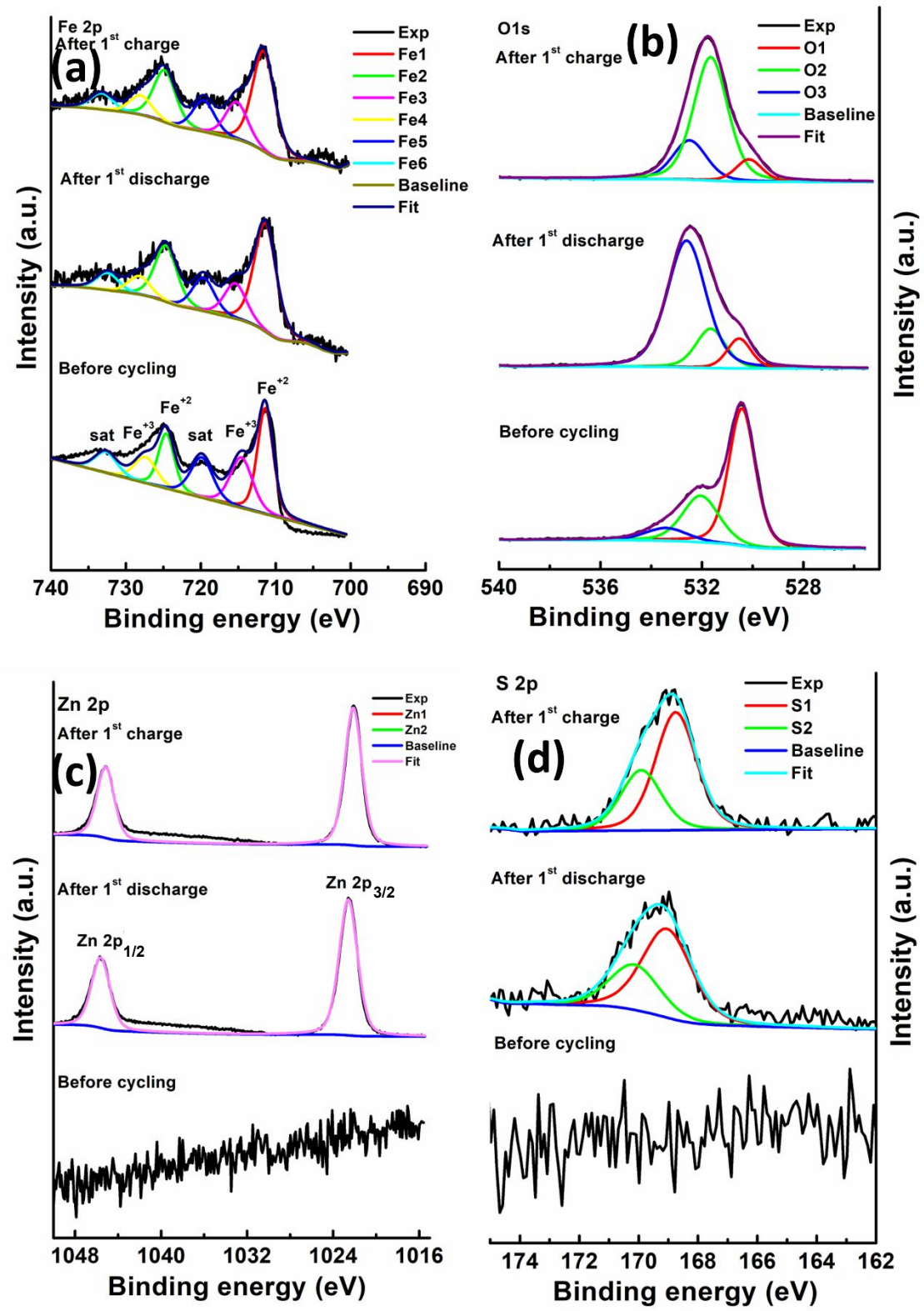

Figure S19: (a-d) XPS spectra of Fe 2p, O1s, Zn 2p, and S 2p of Fe_3O_4-VA-300 electrodes before cycling, after 1st discharge, and 1st charge, respectively (bottom to top).

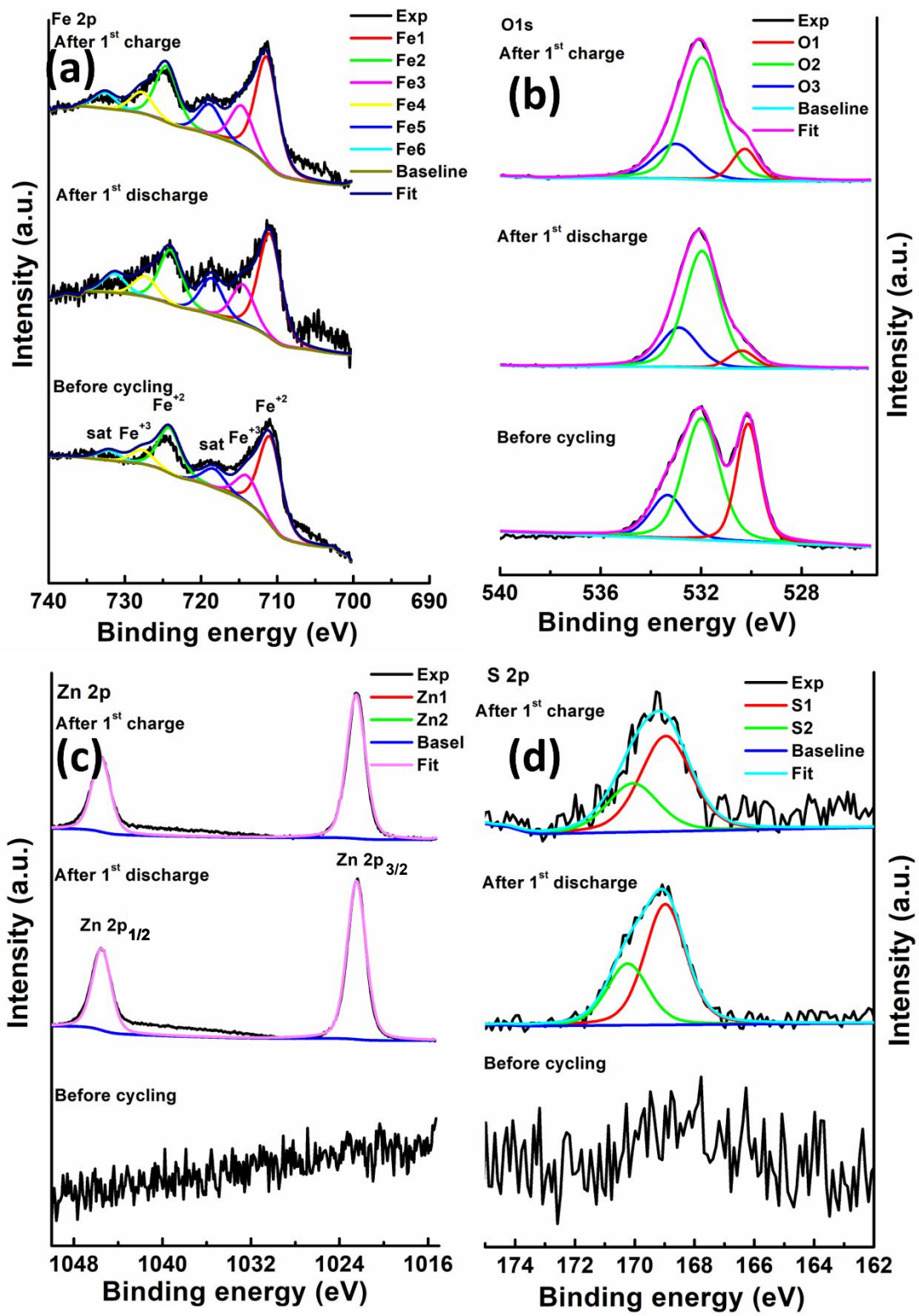

Figure S20: (a-d) XPS spectra of Fe 2p, O1s, Zn 2p, and S 2p of Fe_3O_4-VA-500 electrodes before cycling, after 1st discharge, and 1st charge, respectively (bottom to top).

Table S5: Comparison of XPS results of before and after cycling of the cells and their peak binding energy, FWHM, relative at%, O/Fe, and Fe^{3+}/Fe^{2+} ratios.

State	Composite	Peak binding energy (eV±0.2) / [FWHM (eV)]/ (relative at (%))											Elemental at%				Ratio
		O 1*s*			Fe 2*p*				Zn 2*p*		S 2*p*		O	Fe	Zn	S	Fe^{3+}/Fe^{2+}
					Fe^{2+}		Fe^{3+}										
		O1	O2	O3	Fe1	Fe2	Fe3	Fe4	Zn1	Zn2	S1	S1					
Before Cycling	Pristine Fe_3O_4	530.5 [1.22] (39.91)	532.0 [1.22] (23.92)	533.0 [1.22] (11.55)	711.2 [3.12] (17.28)	724.4	714.3 [3.5] (7.34)	727.6	-	-	-	-	75.38	24.62	-	-	0.42
	Fe_3O_4-VA-300	530.4 [1.23] (45.39)	532.1 [1.23] (21.1)	533.4 [1.23] (6.66)	711.4 [2.5] (16.11)	724.6	714.6 [3.5] (10.74)	727.4	-	-	-	-	73.15	26.85	-	-	0.67
	Fe_3O_4-VA-400	530.4 [1.22] (46.62)	532.0 [1.22] (22.24)	533.3 [1.22] (5.01)	711.1 [2.43] (15.45)	724.4	713.8 [3.5] (10.68)	727.1	-	-	-	-	73.87	26.13	-	-	0.69
	Fe_3O_4-VA-500	530.1 [1.1] (26.27)	532.0 [1.1] (41.67)	533.3 [1.1] (14.11)	710.9 [3.5] (13.69)	724.1	714.0 [3.5] (4.26)	727.7	-	-	-	-	82.05	17.95	-	-	0.31
After 1 Discharge	Pristine Fe_3O_4	530.4 [1.32] (7.13)	531.6 [1.32] (38.47)	532.4 [1.32] (20.95)	710.7 [3.5] (3.26)	723.5	713.6 [3.5] (1.76)	726.7	1022.2 [1.97] (24.04)	1045.2	168.6 [1.47] [4.39]	169.8	66.55	5.02	24.04	4.39	0.53
	Fe_3O_4-VA-300	530.5 [1.12] (8.01)	531.7 [1.12] (12.89)	532.6 [1.12] (53.99)	711.4 [3.5] (3.33)	724.7	715.4 [3.5] (1.09)	728.2	1022.6 [2.02] (17.37)	1045.6	169.1 [1.99] [3.32]	170.1	74.89	4.42	17.37	3.32	0.32
	Fe_3O_4-VA-400	530.5 [1.24] (5.68)	531.9 [1.24] (33.82)	532.7 [1.24] (29.46)	711.1 [3.5] (2.33)	724.2	715.0 [3.5] (0.84)	727.8	1022.5 [1.99] (23.1)	1045.6	168.9 [1.59] [4.77]	170.1	68.96	3.17	23.1	4.77	0.36
	Fe_3O_4-VA-500	530.4 [1.27] (5.33)	532.0 [1.27] (45.62)	532.9 [1.27] (16.18)	711.0 [3.5] (2.5)	724.0	714.5 [3.5] (0.96)	727.3	1022.5 [2.0] (24.76)	1045.5	169.0 [1.62] [4.65]	170.2	67.13	3.46	24.76	4.65	0.38
After 1 charge	Pristine Fe_3O_4	530.0 [1.34] (10.09)	531.3 [1.34] (29.35)	532.0 [1.34] (27.97)	711.3 [3.46] (5.56)	724.6	714.9 [3.5] (2.07)	727.8	1021.9 [1.91] (21.42)	1045.0	168.5 [1.61] [3.54]	169.7	67.41	7.63	21.42	3.54	0.37
	Fe_3O_4-VA-300	530.2 [1.23] (6.55)	531.7 [1.23] (46.99)	532.5 [1.23] (14.84)	711.6 [3.5] (4.6)	724.8	715.2 [3.5] (1.73)	728.0	1022.2 [1.88] (20.52)	1045.2	168.8 [1.63] [4.77]	169.9	68.38	6.33	20.52	4.77	0.38

	Fe_3O_4-VA-400	530.3 [1.19] (5.12)	531.8 [1.19] (40.99)	532.6 [1.19] (20.41)	711.5 [3.5] (3.09)	724.7	715.3 [3.5] (1.19)	728.1	1022.3 [2.01] (24.52)	1045.3	168.8 [1.63] [4.68]	170.1	66.52	4.28	24.52	4.68	0.39
	Fe_3O_4-VA-500	530.3 [1.19] (8.41)	532.0 [1.19] (47.77)	533.0 [1.19] (15.56)	711.4 [3.5] (5.88)	724.5	714.7 [3.5] (2.26)	727.8	1022.5 [2.0] (17.92)	1045.5	169.0 [2.02] [2.2]	170.1	71.74	8.14	17.92	2.2	0.38

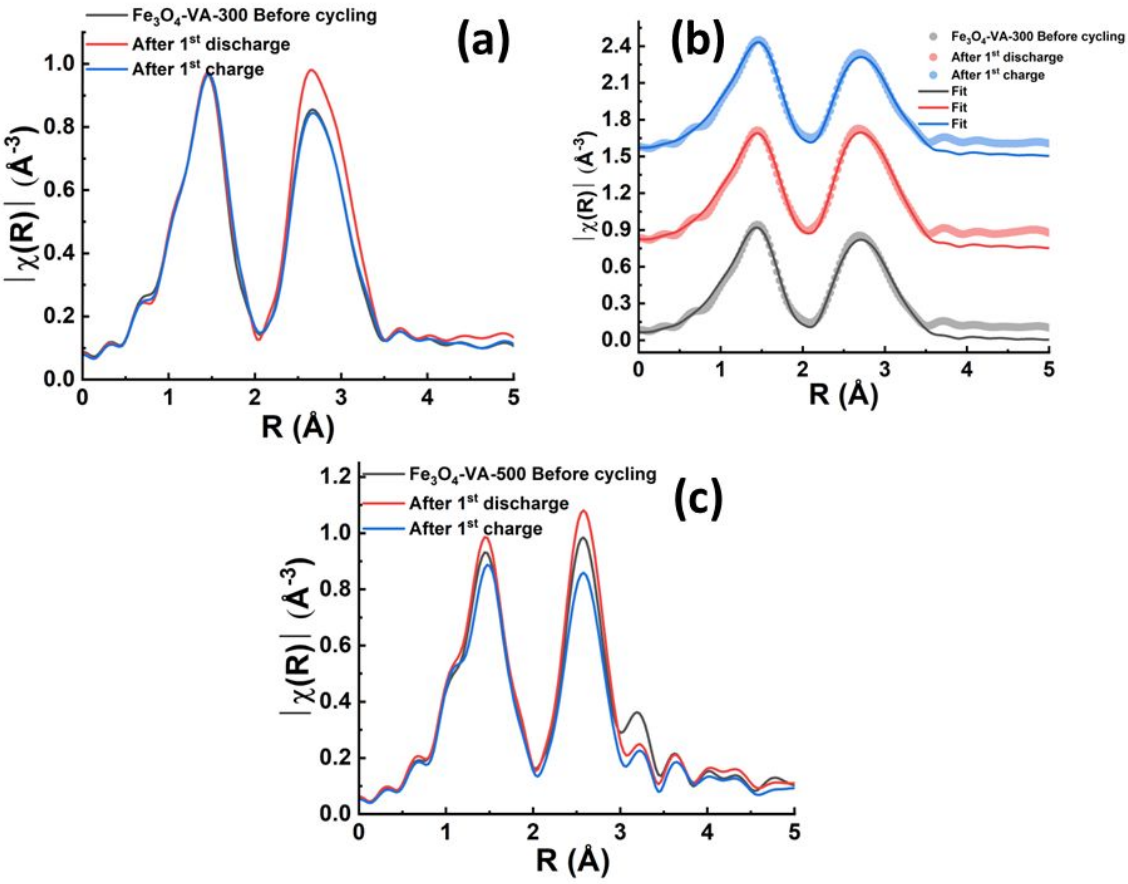

Figure S21: (a and c) Comparison of EXAFS (R-space) data of pristine Fe_3O_4, Fe_3O_4-VA-300, and Fe_3O_4-VA-500 before and after cycling, (b) Experimental EXAFS (R-space) data and the fitting using theoretical model for Fe_3O_4-VA-300.

Table S6: Amplitude reduction factor (S_0^2), correction to edge energy (ΔE_0), coordination number (N), path distance (R), pseudo/EXAFS Debye–Waller factor (σ^2) of the different scattering paths obtained from the EXAFS data fitting of the pristine Fe_3O_4 sample: (A), (B), and (C) – Before cycling, after 1st discharge, and after 1st charge.

R factor = 0.0029

(A) State: Before cycling

Scattering Path	S_0^2	ΔE_0 (eV)	N	R (Å)	σ^2 (Å^2)
Fe – O	0.77	-3.11 ± 0.69	5.95 ± 0.17	1.9661 ± 0.0060	0.0143
$Fe_{Oct} – Fe_{Oct}$	0.77	-3.11 ± 0.69	4.37 ± 0.30	2.9862 ± 0.0071	0.0120
$Fe_{Oct/Tetra} – Fe_{Tetra/Octa}$	0.77	-3.11 ± 0.69	7.89 ± 0.36	3.4725 ± 0.0069	0.0105

(B) State: After 1st discharge

Scattering Path	S_0^2	ΔE_0 (eV)	N	R (Å)	σ^2 (Å^2)
Fe – O	0.77	-3.47 ± 0.82	6.43 ± 0.24	1.9698 ± 0.0073	0.0148
$Fe_{Oct} – Fe_{Oct}$	0.77	-3.47 ± 0.82	4.29 ± 0.36	2.9836 ± 0.0085	0.0110
$Fe_{Oct/Tetra} – Fe_{Tetra/Octa}$	0.77	-3.47 ± 0.82	9.32 ± 0.48	3.4746 ± 0.0082	0.0106

(C) State: After 1st charge

Scattering Path	S_0^2	ΔE_0 (eV)	N	R (Å)	σ^2 (Å^2)
Fe - O	0.77	-2.80 ± 0.78	6.17 ± 0.19	1.9692 ± 0.0067	0.0141
$Fe_{Oct} – Fe_{Oct}$	0.77	-2.80 ± 0.78	4.81 ± 0.37	2.9894 ± 0.0081	0.0126
$Fe_{Oct/Tetra} – Fe_{Tetra/Octa}$	0.77	-2.80 ± 0.78	8.12 ± 0.42	3.4745 ± 0.0077	0.0106

Table S7: Fitting results (S_0^2, ΔE_0, N, R, and σ^2) obtained from the EXAFS data fitting of the Fe_3O_4-VA-300sample: (A), (B), and (C) – Before cycling, after 1st discharge, and after 1st charge.

R factor = 0.0035

(A) State: Before cycling

Scattering Path	S_0^2	ΔE_0 (eV)	N	R (Å)	σ^2 (Å^2)
Fe - O	0.77	-4.12 ± 0.97	5.46 ± 0.17	1.9343 ± 0.0074	0.0119
$Fe_{Oct} - Fe_{Oct}$	0.77	-4.12 ± 0.97	4.02 ± 0.41	2.9831 ± 0.0089	0.0132
$Fe_{Oct/Tetra} - Fe_{Tetra/Octa}$	0.77	-4.12 ± 0.97	7.35 ± 0.49	3.4455 ± 0.0093	0.0119

(B) State: After 1st discharge

Scattering Path	S_0^2	ΔE_0 (eV)	N	R (Å)	σ^2 (Å^2)
Fe - O	0.77	-3.39 ± 0.85	6.12 ± 0.19	1.9466 ± 0.0069	0.0133
$Fe_{Oct} - Fe_{Oct}$	0.77	-3.39 ± 0.85	4.24 ± 0.37	2.9855 ± 0.0081	0.0119
$Fe_{Oct/Tetra} - Fe_{Tetra/Octa}$	0.77	-3.39 ± 0.85	8.09 ± 0.46	3.4586 ± 0.0084	0.0111

(C) State: After 1st charge

Scattering Path	S_0^2	ΔE_0 (eV)	N	R (Å)	σ^2 (Å^2)
Fe - O	0.77	-2.45 ± 1.08	5.94 ± 0.21	1.9575 ± 0.0086	0.0129
$Fe_{Oct} - Fe_{Oct}$	0.77	-2.45 ± 1.08	5.16 ± 0.53	3.0038 ± 0.0104	0.0148
$Fe_{Oct/Tetra} - Fe_{Tetra/Octa}$	0.77	-2.45 ± 1.08	5.98 ± 0.50	3.4627 ± 0.0100	0.0106

Table S8: Fitting results (S_0^2, ΔE_0, N, R, and σ^2) obtained from the EXAFS data fitting of the Fe_3O_4-VA-400 sample: (A), (B), and (C) – Before cycling, after 1st discharge, and after 1st charge.

R factor = 0.0041

(A) State: Before cycling

Scattering Path	S_0^2	ΔE_0 (eV)	N	R (Å)	σ^2 (Å^2)
Fe - O	0.77	-4.38 ± 1.04	5.46 ± 0.19	1.9329 ± 0.0080	0.0122
$Fe_{Oct} - Fe_{Oct}$	0.77	-4.38 ± 1.04	3.53 ± 0.37	2.9731 ± 0.0094	0.0119
$Fe_{Oct/Tetra} - Fe_{Tetra/Octa}$	0.77	-4.38 ± 1.04	6.59 ± 0.51	3.4402 ± 0.0105	0.0119

(B) State: After 1st discharge

Scattering Path	S_0^2	ΔE_0 (eV)	N	R (Å)	σ^2 (Å^2)
Fe - O	0.77	-4.31 ± 1.02	6.18 ± 0.22	1.9427 ± 0.0081	0.0132
$Fe_{Oct} - Fe_{Oct}$	0.77	-4.31 ± 1.02	4.12 ± 0.43	2.9787 ± 0.0094	0.0118
$Fe_{Oct/Tetra} - Fe_{Tetra/Octa}$	0.77	-4.31 ± 1.02	8.59 ± 0.58	3.4509 ± 0.0100	0.0118

(C) State: After 1stcharge

Scattering Path	S_0^2	ΔE_0 (eV)	N	R (Å)	σ^2 (Å^2)
Fe - O	0.77	-3.59 ± 1.06	5.94 ± 0.21	1.9547 ± 0.0083	0.0127
$Fe_{Oct} - Fe_{Oct}$	0.77	-3.59 ± 1.06	5.26 ± 0.52	2.9972 ± 0.0100	0.0147
$Fe_{Oct/Tetra} - Fe_{Tetra/Octa}$	0.77	-3.59 ± 1.06	6.34 ± 0.51	3.4582 ± 0.0099	0.0110

Table S9: Lattice parameter obtained from the EXAFS data fitting (in Å).

State	Sample		
	Pristine-Fe_3O_4	**Fe_3O_4-VA-300**	**Fe_3O_4-VA-400**
Before cycling	8.45(2)	8.44(3)	8.41(3)
After 1stdischarge	8.44(2)	8.44(2)	8.43(3)
After 1st charge	8.46(2)	8.50(3)	8.48(3)

Table S10: Density functional theory (DFT) calculated reaction enthalpies, represented as voltages versus Zn metal, for possible conversion reactions of Zn with stoichiometric Fe_3O_4 and intercalation into Fe-deficient $Fe_{22}O_{32}$. Voltage for a given reaction equals the negative of reaction enthalpy (in eV) normalized by the 2 × number of Zn atoms as a reactant and the Faraday constant. Positive reaction voltage indicates spontaneity. Reactions in bold are most spontaneous.

Reaction	**Calculated reaction voltage (V vs. Zn)**
$Zn + Fe_3O_4 \rightarrow ZnFe_2O_4 + Fe$	0.22
$Zn + Fe_3O_4 \rightarrow ZnO + 3FeO$	0.19
$Zn + 2Fe_3O_4 \rightarrow ZnO + Fe_2O_3 + 4FeO$	0.02
$Zn + 2Fe_3O_4 \rightarrow ZnFe_2O_4 + 4FeO$	0.01
$Zn + 2Fe_3O_4 \rightarrow ZnFe_2O_4 + Fe_2O_3 + FeO + Fe$	0.05
$Zn + 4Fe_3O_4 \rightarrow ZnFe_2O_4 + 2Fe_2O_3 + 6FeO$	-0.34
$4Zn + Fe_3O_4 \rightarrow 4ZnO + 3Fe$	**0.35**
$2Zn + Fe_3O_4 \rightarrow 2ZnO + 2FeO + Fe$	0.30
$Zn + Fe_3O_4 \rightarrow ZnO + Fe_2O_3 + Fe$	0.23
$Zn + 2Fe_3O_4 \rightarrow ZnO + 2Fe_2O_3 + FeO + Fe$	0.06
$2Zn + 3Fe_3O_4 \rightarrow ZnO + ZnFe_2O_4 + 7FeO$	0.10
$Zn + 3Fe_3O_4 \rightarrow ZnFe_2O_4 + Fe_2O_3 + 5FeO$	-0.16
$4Zn + 5Fe_3O_4 \rightarrow 4ZnO + 4Fe_2O_3 + 4FeO + 3Fe$	0.18
$2Zn + 4Fe_3O_4 \rightarrow ZnO + ZnFe_2O_4 + Fe_2O_3 + 8FeO$	0.01
$2Zn + 2Fe_3O_4 \rightarrow ZnO + ZnFe_2O_4 + Fe_2O_3 + 2Fe$	0.22
$4Zn + 3Fe_3O_4 \rightarrow 2ZnO + 2ZnFe_2O_4 + 2FeO + 3Fe$	0.26
$8Zn + 5Fe_3O_4 \rightarrow 4ZnO + 4ZnFe_2O_4 + 7Fe$	0.28
$2Zn + 8Fe_3O_4 \rightarrow Zn_2Fe_{22}O_{32} + 2Fe$	-0.75
$2Zn + Fe_{22}O_{32} \rightarrow Zn_2Fe_{22}O_{32}$ (intercalation)	**0.86**